RSC Advances

PAPER

View Article Online
View Journal | View Issue

Cite this: *RSC Adv.*, 2018, **8**, 33972

Magnetic core–shell-structured Fe_3O_4@CeO_2 as an efficient catalyst for catalytic wet peroxide oxidation of benzoic acid†

Hangdao Qin, *[a] Rong Xiao,[b] Wei Shi,[a] Yong Wang,[a] Hui Li,[a] Lei Guo,[a] Hao Cheng[a] and Jing Chen[a]

Received 27th August 2018
Accepted 18th September 2018

DOI: 10.1039/c8ra07144f

rsc.li/rsc-advances

A magnetic core–shell-structured Fe_3O_4@CeO_2 catalyst was prepared by a simple solvothermal method and applied in the solid state for catalytic wet peroxide oxidation (CWPO) of benzoic acid. The obtained catalyst was characterized by N_2 adsorption–desorption, X-ray diffraction (XRD), magnetic measurements, transmission electron microscopy (TEM) and X-ray photoelectron spectroscopy (XPS). The experimental results showed that Fe_3O_4@CeO_2 possessed superior catalytic efficiency for CWPO of benzoic acid than that of Fe_3O_4. The high catalytic activity was caused by a synergistic effect between Fe_3O_4 and CeO_2, which assisted the decomposition of H_2O_2 into hydroxyl radicals (·OH). Fe_3O_4@CeO_2 exhibited low Fe leaching of 4.2 mg L^{-1}, which approximately accounted for barely 0.76% of the total Fe amount in the catalyst. The effects of radical scavengers indicated that benzoic acid was degraded mainly by ·OH attack, which occurred both in the bulk solution and on the Fe_3O_4@CeO_2 surface. In the stability tests, there was loss of merely 4% in the benzoic acid removal rate after six cycles of reaction, and the saturation magnetization of Fe_3O_4@CeO_2 hardly changed, which suggested that the Fe_3O_4@CeO_2 catalyst was fairly effective in reutilization and stability.

1. Introduction

Benzoic acid is well-known for its wide range of applications in food preservatives and reaction intermediates,[1] but wastewater containing benzoic acid in manufacturing industries can be highly toxic and harmful. Traditional processes such as biological treatments have negligible effect on benzoic acid due to its low biodegradability. Other approaches including adsorption,[2,3] photocatalytic degradation[4,5] and chemical oxidation[6] have also been extensively investigated to remove benzoic acid from aqueous solutions. Among the advanced oxidation processes, catalytic wet peroxide oxidation (CWPO) has attracted increasing attention due to its low cost, ambient reaction conditions, and nontoxic products from H_2O_2 decomposition.[7,8]

As favorable catalysts for CWPO, iron-based materials can initiate a modified Fenton process over solid surfaces by heterogeneously catalyzing the degradation of organics.[9–13] During this process, H_2O_2 is decomposed effectively into ·OH, and the radicals then react rapidly with organics along with their intermediates. Some metals with multiple redox states other than Fe-containing catalysts, such as Mn, Cu, and Ce, can also function as Fenton-like catalysts with similar catalytic mechanisms to that of the iron-based ones.[14–16]

An important but inexpensive rare earth oxide, cerium oxide, demonstrates broad applications in developed oxidation processes either as a catalyst or as a non-inert support for catalysts.[17–20] Both the presence of oxygen vacancies on the oxide surface and the availability of surface Ce^{3+} at such defect sites can contribute to excellent catalytic activity. Fe_3O_4/CeO_2 composite particles were prepared *via* an impregnation method and applied as Fenton-like catalysts for 4-chlorophenol degradation.[21] Compared with isolated Fe_3O_4 or CeO_2, the obtained composites exhibited higher catalytic activity, suggesting the existence of a certain synergistic effect between these two metal oxides. The thermodynamically favored electron transfer from Fe^{2+} to Ce^{4+} resulted in increasing Ce^{3+} ions during the CWPO reaction process, whereas serious iron leaching up to 11.8 mg L^{-1} occurred in the meantime.

Magnetic catalysts with a core–shell structure have received increasing attention these days as they can prevent undesired aggregation and metal leaching while maintaining the necessary stability and reusability.[22–24] Moreover, the magnetic property of Fe_3O_4 is conducive to recover the catalyst from solution, which plays an important role in practical applications. On this basis, further investigation was carried out for the usage of magnetic core–shell-structured cerium oxide for CWPO reactions. Here, magnetic core–shell-structured Fe_3O_4@CeO_2 nanoparticles were successfully prepared and subsequently

[a]*School of Material and Chemical Engineering, Tongren University, Tongren 554300, China. E-mail: qinhangdao@126.com; Fax: +86-856-5225621; Tel: +86-856-5225621*
[b]*School of Pharmacy, Tongren Polytechnic College, Tongren 554300, China*

† Electronic supplementary information (ESI) available. See DOI: 10.1039/c8ra07144f

characterized using N_2 adsorption–desorption, X-ray diffraction (XRD), magnetic measurements, transmission electron microscopy (TEM), and X-ray photoelectron spectroscopy (XPS). Their performance with respect to adsorption and CWPO of benzoic acid was evaluated by examining the benzoic acid and TOC removal. The influences of initial solution pH and radical scavengers on the degradation rate of benzoic acid during the CWPO process were systematically studied, whereas leaching of iron and cerium from the catalyst into aqueous solution was measured as well. The possible catalysis mechanism of Fe_3O_4@CeO_2 in the CWPO process was thus proposed according to the results of above-mentioned analyses. Finally, the stability of the Fe_3O_4@CeO_2 catalyst was tested with six successive runs.

2. Experimental

2.1. Catalyst preparation

Fe_3O_4 and CeO_2 nanoparticles were obtained from Sigma-Aldrich. The commercially obtained Fe_3O_4 and CeO_2 particles were uniform with a diameter of around 100 nm. Core–shell-structured Fe_3O_4@CeO_2 nanoparticles were synthesized referring to the following description.[25] First, a ceria precursor solution was prepared by the solvothermal method; 1 g $Ce(NO_3)_3 \cdot 6H_2O$ and 1 g NaOH were separately dissolved in 20 mL of ethanol, and the mixture was stirred vigorously at a constant temperature of 50 °C for 24 h. Then, 0.05 mL of 30% H_2O_2 was added to the mixture solution under continuous stirring for 2 h. The precipitate was collected by centrifugation and washed before drying at 60 °C for 4 h. Under continuous stirring, 1 g of precipitate was then dispersed in 20 mL distilled water. The pH of the solution was adjusted to 0.1 using concentrated nitric acid. After stirring for 2 h, the ceria precursor solution was obtained when the solution was cooled to room temperature naturally. Afterwards, 0.1 g of Fe_3O_4 nanoparticles was dispersed in a mixture containing 30 mL distilled water and 3 mL of ceria precursor solution through an ultrasonic treatment process for 15 min. Also, 0.5 mol L^{-1} ammonium hydroxide solution was added to adjust the pH to 6.8. The final mixed solution was agitated vigorously by stirring for 4 h at 60 °C. After the reaction was completed, the particles were collected using an external magnet, washed thoroughly with ethanol, and dried in a vacuum oven at 60 °C overnight. The final products were obtained by heat treatment of the particles in a tube furnace under N_2 flow, which lasted for 3 h at 300 °C with a heating rate of 3 °C min^{-1}.

X-ray powder diffraction (XRD) was conducted on a Philips X'Pert MPD diffractometer using Cu Kα radiation. The specific surface area and pore volume of catalysts were calculated from N_2 adsorption and desorption isotherms at −196 °C, which were acquired using a Builder SSA-420 instrument. Samples should be *in vacuo* outgassed at 300 °C overnight prior to the measurements. Magnetic testing was carried out on the VSM Digital Measurement System JDM-13 by applying a vibrating sample magnetometer. The morphology and structure of the prepared catalysts were observed and characterized by transition electron microscopy (TEM, JEOL model JEM-2010, acceleration voltage 200 kV) with samples suspended in ethanol and dropped on copper grids with a holey-carbon film support. X-ray photoelectron spectroscopy (XPS) was performed on a Kratos XSAM800 spectrometer with monochromatic Al Kα as the radiation source, and all binding energies were calibrated by the C 1s peak at 284.6 eV. XPS data of Ce 3d and Fe 2p spectra were fitted using the software CasaXPS.

2.2. Oxidation experiments

Oxidation was conducted in a 250 mL jacketed glass reactor equipped with a magnetic stirrer. In each operation, the reactor was first filled with benzoic acid solution (100 mL, initial concentration 50 mg L^{-1}), followed by adjusting the initial pH to set values with 0.1 mol L^{-1} HCl or 0.1 mol L^{-1} NaOH solution. The reaction temperature was set as 30 °C, which was maintained constant with water circulation in the thermostatic bath provided by the jacket. Then, a certain volume of 30% H_2O_2 (the theoretically stoichiometric amount required for complete mineralization of benzoic acid) and 100 mg of catalyst were added simultaneously to initiate the reaction. For adsorption experiments, the H_2O_2 solution was replaced by deionized water of identical volume. Samples were periodically extracted and immediately filtered with a 0.45 μm membrane for further analyses, whereas the residual H_2O_2 was consumed by adding sodium hydrogen sulfite. Each experiment was run three times, and the average value was reported.

2.3. Analytical techniques

The concentration of benzoic acid was evaluated by a high performance liquid chromatograph (HPLC, Shimadzu Prominence LC-20A) equipped with a UV detector and a C18 reverse phase column (4.6 × 250 mm, 5 μm). The mobile phase was methanol/ammonium acetate (5/95), flow rate was 1.0 mL min^{-1}, injection volume was 10 μL, and detection wavelength was 230 nm. The solution pH was monitored by a PHC-3C pH meter. The leaching amount of Fe and Ce from Fe_3O_4@CeO_2 catalyst to the solution during oxidation was determined by inductively coupled plasma atomic emission spectrometry (ICP-AES, ICPE-9000, Thermo Electron Corporation, USA). The total organic carbon (TOC) was measured using a Shimadzu TOC-5000A analyzer.

3. Results and discussion

3.1. Characterization of catalysts

The crystal structures of nanoparticles were examined by XRD, and the XRD pattern of Fe_3O_4@CeO_2 nanoparticles is shown in Fig. 1a. The diffraction peaks for Fe_3O_4@CeO_2 can be clearly discerned at 30.2°, 35.5°, 36.8°, 43.2°, 53.5°, 57.2°, and 62.7°, which correspond to the lattice planes of (220), (311), (222), (400), (422), (511), and (440).[26] Diffraction peaks assigned to CeO_2 with a cubic fluorite structure appear at 28.6°, 33.1°, 47.6° and 56.5°, which correspond to the lattice planes of (111), (200), (220) and (311).[17]

The physical and chemical properties of Fe_3O_4, CeO_2 and Fe_3O_4@CeO_2 nanoparticles are summarized in Table 1. The Brunauer–Emmett–Teller surface area (S_{BET}), pore size, and

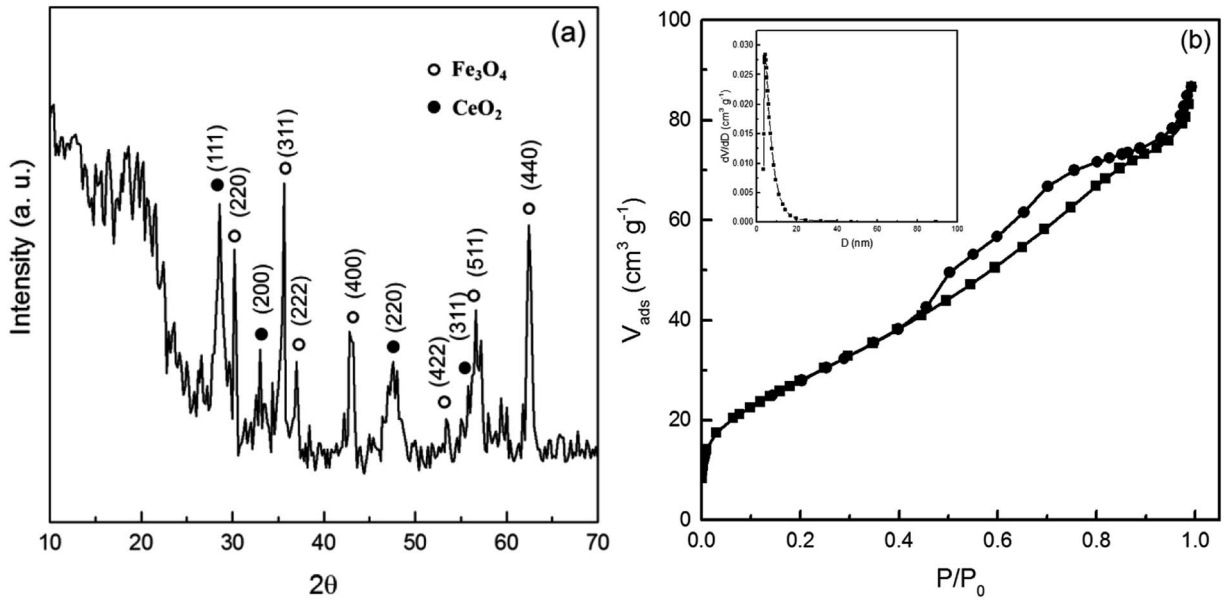

Fig. 1 (a) X-ray pattern of Fe_3O_4@CeO_2 nanoparticles; (b) N_2 adsorption–desorption isotherms and pore size distribution (inset) of Fe_3O_4@CeO_2 nanoparticles.

pore volume of Fe_3O_4 were 65.6 m^2 g^{-1}, 0.026 cm^3 g^{-1}, and 5.19 nm, respectively. CeO_2 covering the Fe_3O_4 surface enhanced both the surface area and pore volume, which was due to the existence of large channels resulting from CeO_2 deposition in the coating layer. Besides, as presented in Fig. 1b, the N_2 adsorption–desorption isotherm of Fe_3O_4@CeO_2 was type IV accompanied with an apparent type H3 hysteresis loop, indicating a mesoporous structure.[27] The corresponding pore size distribution (inset of Fig. 1b) further confirmed such a structure.

The room temperature magnetization curves of Fe_3O_4 and Fe_3O_4@CeO_2 nanoparticles are presented in Fig. S1 of the ESI.† Superparamagnetic properties were observed for both types of nanoparticles with nearly zero coercivity and remanence. The saturation magnetization (M_s) values were 69.1 and 22.9 emu g^{-1} for Fe_3O_4 and Fe_3O_4@CeO_2 nanoparticles, respectively. The lower M_s value for Fe_3O_4@CeO_2 was mainly ascribed to the existence of CeO_2.[25] As shown in the inset of Fig. S1,† the core–shell-structured Fe_3O_4@CeO_2 nanoparticles were proven to be a promising candidate for the removal of organic contaminants as suggested by the easy separation from reaction solution under an external magnetic field due to the magnetic nature.

Fig. 2 presents the morphology of Fe_3O_4@CeO_2 nanoparticles with particle sizes listed in Table 1. Fig. 2a demonstrates the regularity and uniformity of the obtained Fe_3O_4@CeO_2 nanoparticles with diameters ranging from 100 nm to 150 nm; CeO_2 nanoparticles were well dispersed on the surface of Fe_3O_4 nanocrystals with negligible aggregation. The lattice fringe spacing of the nanoparticles (Fig. 2b) was about 0.25 nm, corresponding to the (311) reflection plane with a diffraction peak at 35.5°. The lattice fringe spacing of Fe_3O_4@CeO_2 was about 0.32 nm, which could be assigned to the (111) reflection plane of CeO_2 with the diffraction peak at 28.6° (Fig. 1a).

Ce 3d and Fe 2p peaks were analyzed in detail by XPS for better understanding of the chemical states of Ce and Fe in Fe_3O_4@CeO_2. XPS spectra for Fe_3O_4@CeO_2 before and after reaction are given in Fig. 3. The Ce 3d region could be resolved into eight peaks; peaks v_1 and u_1 were ascribed to Ce^{3+}, whereas other peaks were assigned to Ce^{4+}.[17,21,25] The reaction with H_2O_2 led to larger v_1 and u_1 peaks (Fig. 3b), which indicated the increasing amount of Ce^{3+} on the Fe_3O_4@CeO_2 surface.

Fe 2p spectra in both Fig. 3c and d display a spin–orbit doublet with binding energies of 723.6 eV for Fe $2p_{1/2}$ and 709.8 eV for Fe $2p_{3/2}$. The Fe $2p_{3/2}$ peak was deconvoluted into two parts in terms of an Fe^{2+} peak at 709.0 eV and Fe^{3+} peak at 711.0 eV.[21,28] After reacting for 120 min, a decreased peak area for Fe^{2+} was observed, implying the oxidation of Fe^{2+} to Fe^{3+} by H_2O_2 on the surface of Fe_3O_4@CeO_2.

3.2. Catalytic activity of catalysts

The removal efficiencies of benzoic acid among varied processes were compared (initial benzoic acid concentration of

Table 1 Physical and chemical properties of Fe_3O_4 and Fe_3O_4@CeO_2 nanoparticles

Sample	S_{BET} (m^2 g^{-1})	Pore volume (cm^3 g^{-1})	Average pore size (nm)	M_s (emu g^{-1})	Particle size (nm)
Fe_3O_4	65.6	0.026	5.19	69.1	100
CeO_2	85.6	0.041	5.12	—	100
Fe_3O_4@CeO_2	104.9	0.15	4.49	22.9	100–150

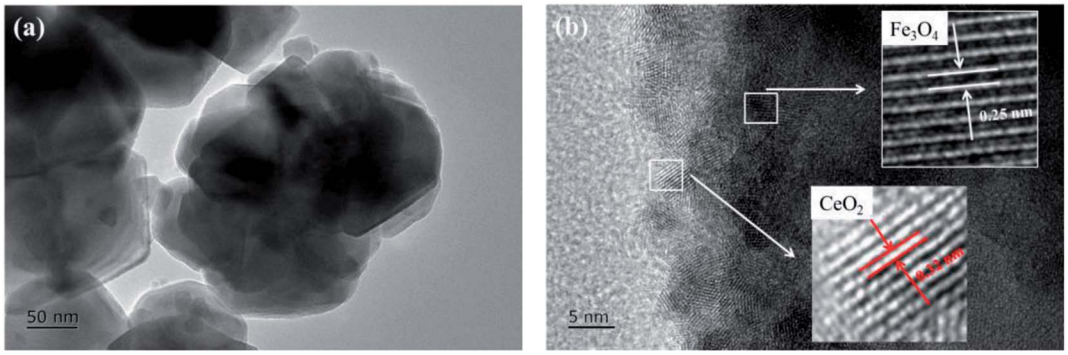

Fig. 2 TEM and HR-TEM images of Fe_3O_4@CeO_2.

50 mg L^{-1}) to investigate the catalytic activity of Fe_3O_4@CeO_2 in benzoic acid CWPO. As shown in Fig. 4a, the removal efficiency was approximately 10% after 120 min of reaction without catalyst; in other words, it was difficult to degrade benzoic acid by H_2O_2 alone. On the other hand, about 4%, 3%, and 6% removal was observed for Fe_3O_4, CeO_2, and Fe_3O_4@CeO_2 alone

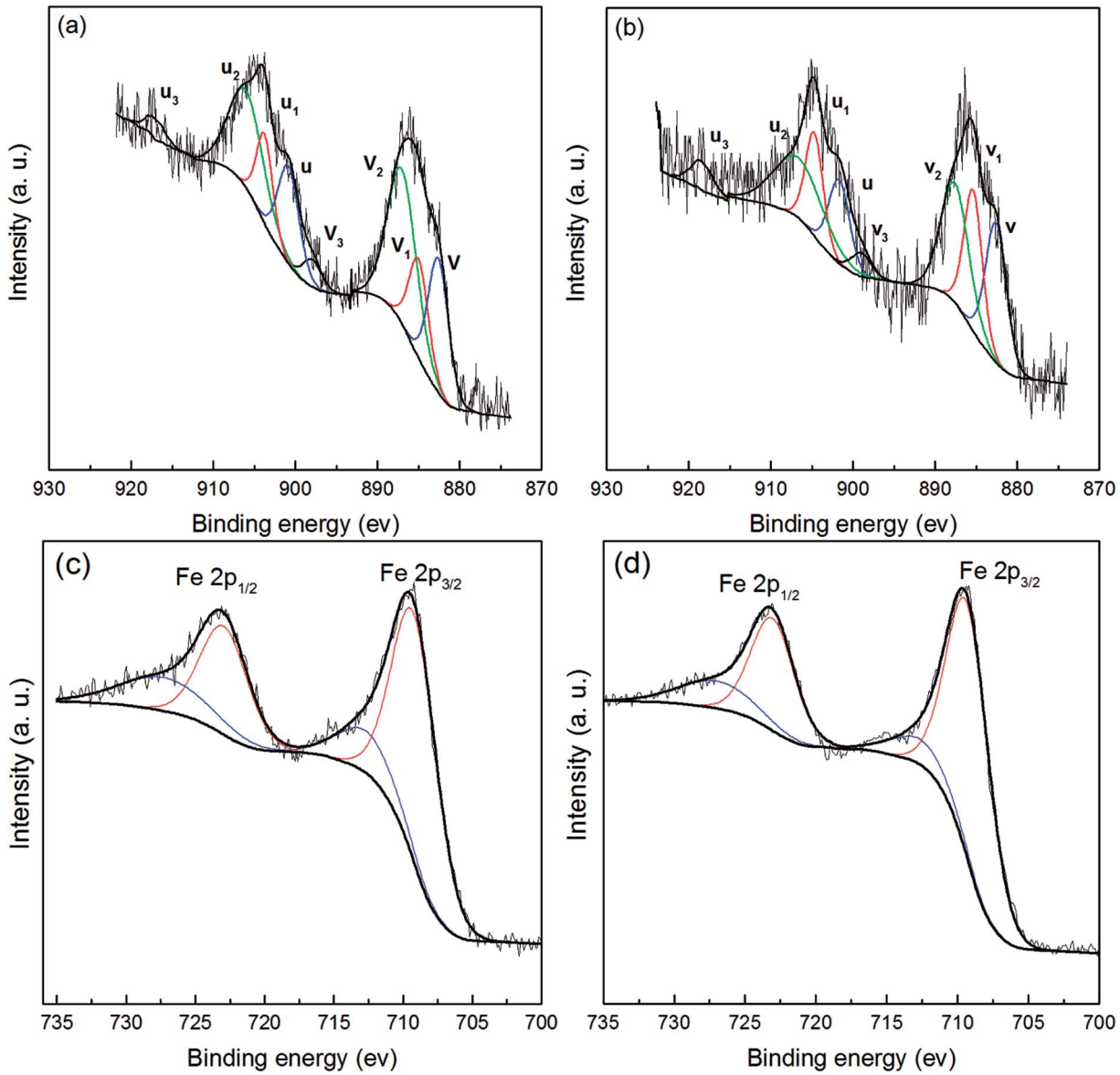

Fig. 3 (a) Ce 3d and (c) Fe 2d XPS spectra of Fe_3O_4@CeO_2 before reaction; (b) Ce 3d and (d) Fe 2d XPS spectra of Fe_3O_4@CeO_2 after reaction.

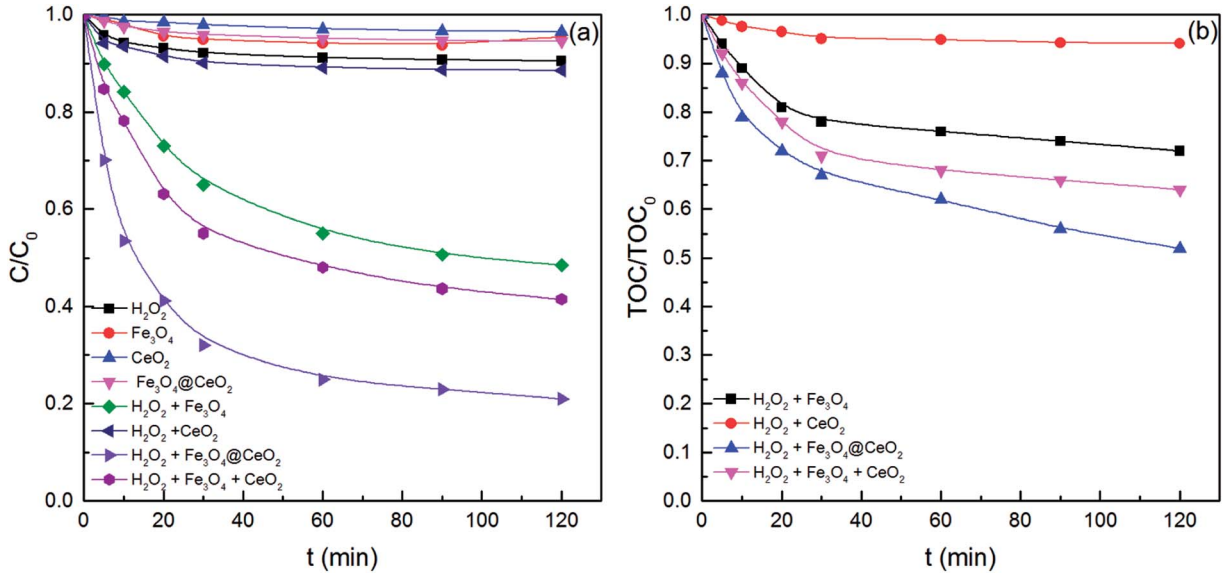

Fig. 4 Removal efficiency of (a) benzoic acid and (b) TOC in different processes. Experimental conditions: 50 mg L^{-1} of benzoic acid, 1 g L^{-1} of catalyst, 250 mg L^{-1} of H_2O_2, $T = 30$ °C, pH = 3.2.

primarily due to surface adsorption, which was almost negligible compared to the fast removal in the CWPO reaction. In the CWPO process, a small amount of benzoic acid degraded in the presence of pure CeO_2. The removal efficiency with Fe_3O_4@CeO_2 as the catalyst became notably higher than that for pure Fe_3O_4, indicating that the catalytic activity was enhanced by CeO_2 coating. Moreover, the degradation of benzoic acid by a physical mixture of Fe_3O_4 and CeO_2 materials (concentration of 1 g L^{-1} and mass ratio of 1 : 1) was also examined. The catalytic performance of Fe_3O_4@CeO_2 was higher that of the physical mixture of Fe_3O_4 and CeO_2 materials, which suggested that a synergistic effect might exist between Fe_3O_4 and CeO_2 in Fe_3O_4@CeO_2 nanoparticles.[29]

Fig. 4b depicts the TOC removal trend during benzoic acid degradation by CWPO. As can be seen, the mineralization degree was 48% after 120 min of reaction in the presence of Fe_3O_4@CeO_2, whereas the removal rate of benzoic acid reached 80% under the same conditions. Such phenomena suggested the remainder of several intermediates that formed during oxidation in the solution such as small chain carboxylic acids. Besides, the best TOC removal performance exhibited by Fe_3O_4@CeO_2 could be explained by the synergetic effect of Fe_3O_4 and CeO_2 that accelerated ·OH generation and induced deeper oxidation of intermediates.[29]

3.3. Effect of initial pH

Since CWPO is a strongly pH-dependent process, we further studied how the initial solution pH can influence benzoic acid degradation with Fe_3O_4@CeO_2 as a catalyst. Fe_3O_4@CeO_2 could function over a wide pH range, as suggested by the degradation efficiency of benzoic acid up to 80% at both acidic and neutral pH (Fig. 5). Nevertheless, further increase in solution pH reduced the removal rate of benzoic acid as the rapid decomposition of H_2O_2 in alkaline solution (pH 8.5 and 10.3 in this case) could generate molecular oxygen rather than ·OH; molecular oxygen is incapable of efficiently oxidizing organics under mild conditions.[21,29] As a result, the lowest removal rate of benzoic acid was shown at pH 10.3.

3.4. Metal leaching

The concentrations of leached Fe and Ce in solution during CWPO of benzoic acid were monitored at an initial pH of 3.2, and dissolved Ce was hardly detected due to cerium oxide's insolubility in water.[30,31] As shown in Fig. 6, the total concentration of Fe leaching was 4.2 mg L^{-1}, which barely accounted

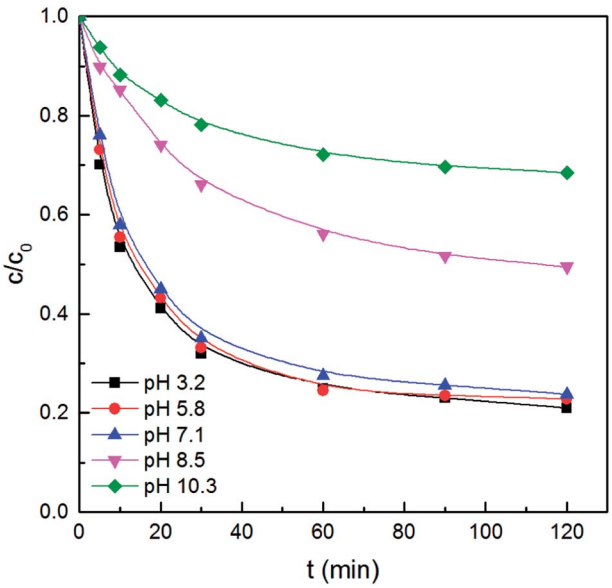

Fig. 5 Effect of solution pH on the degradation of benzoic acid in CWPO with Fe_3O_4@CeO_2 catalyst. Experimental conditions: 50 mg L^{-1} of benzoic acid, 1 g L^{-1} of catalyst, 250 mg L^{-1} of H_2O_2, $T = 30$ °C.

for 0.76% of Fe content in the original Fe_3O_4@CeO_2 catalyst. The leaching level of Fe in this study was much lower than the reported value for Fe_3O_4/CeO_2 composites prepared by the impregnation method.[21]

The variation of Fe^{2+} concentration is given in Fig. 6, where a tendency to increase first and then decrease was observed. The concentration of Fe^{2+} increased and then reached a peak value of about 1.8 mg L^{-1} at 60 min when the degradation rate of benzoic acid no longer sharply increased. As the oxidation reaction progressed, the concentration of Fe^{2+} decreased to about 0.6 mg L^{-1} after 120 min of the reaction. Similar results were reported in previous studies.[32,33] In the ascending stage, the oxidation of the Fe_3O_4@CeO_2 catalyst by H_2O_2 could release Fe^{2+} into solution.[16,21] Fe^{2+} in the aqueous solution played an important role in the decomposition of H_2O_2 and the generation of ·OH. In the descending stage, dissolved Fe^{2+} was oxidized to Fe^{3+} by the remaining H_2O_2. Accordingly, the total leached Fe increased the entire time, which could be ascribed to the leaching of Fe^{2+} and Fe^{3+} from the Fe_3O_4@CeO_2 catalyst as well as the oxidation of Fe^{2+} in solution.

3.5. Possible catalysis mechanism of Fe_3O_4@CeO_2

To verify the actual reactive species mediated in the CWPO process, the effect of *tert*-butanol and KI as radical scavengers on the degradation of benzoic acid was investigated. *tert*-Butanol has a fast reaction rate with ·OH and can terminate radical chain reactions; iodide ions can eliminate surface-bound ·OH (·OH_s) produced at the surface of the Fe_3O_4@CeO_2 catalyst.[21,26]

It can be seen from Fig. 7 that the degradation rate decreased by about 61.5% in the presence of 300 mmol L^{-1} *tert*-butanol, which implied significant influence of ·OH reaction on benzoic acid decomposition. Compared to the result for single H_2O_2 oxidation, the removal efficiency obtained in the presence of *tert*-butanol increased by about 6%, which could be due to the adsorption of Fe_3O_4@CeO_2 (Fig. 4a). Moreover, with the addition of 10 mmol L^{-1} KI, the benzoic acid degradation rate decreased from 80% (in the absence of KI) to 62% after 120 min of the reaction, suggesting that surface reactions involving ·OH_s play a considerable role in benzoic acid degradation.[16,21]

On the basis of the results obtained above, it could be concluded that benzoic acid degradation occurred both in the bulk solution and on the catalyst surface. A possible catalysis mechanism of core–shell-structured Fe_3O_4@CeO_2 in CWPO was proposed. As proposed by other researchers,[34] the existing Ce^{3+} on the surface of the CeO_2 shell could react with H_2O_2 to produce surface-bound ·OH_s, and Ce^{3+} was simultaneously oxidized to Ce^{4+}. When H_2O_2 diffused from the bulk solution to the surface of the Fe_3O_4 core through the channels of CeO_2, the existing Fe^{2+} reacted with H_2O_2 to generate ·OH_s,[35–37] which could explain why the amount of Fe^{2+} on the Fe_3O_4@CeO_2 surface determined by XPS decreased after the CWPO reaction (Fig. 3). Some produced ·OH_s species reacted with benzoic acid on the catalyst surface, and the rest diffused from the catalyst surface into the bulk solution. Furthermore, the transfer of electrons from Fe^{2+} to Ce^{4+} occurred, and the amount of Ce^{3+} on the catalyst surface increased after the CWPO reaction, which was confirmed by the results of XPS (Fig. 3). Similar to Fe^{2+} on the catalyst surface, the leached Fe^{2+} in bulk solution initiated the decomposition of H_2O_2 to produce ·OH for the oxidation of benzoic acid and other intermediates.

3.6. Stability tests

The stability of the Fe_3O_4@CeO_2 catalyst is an important factor for potential industrial applications. To evaluate recyclability, the

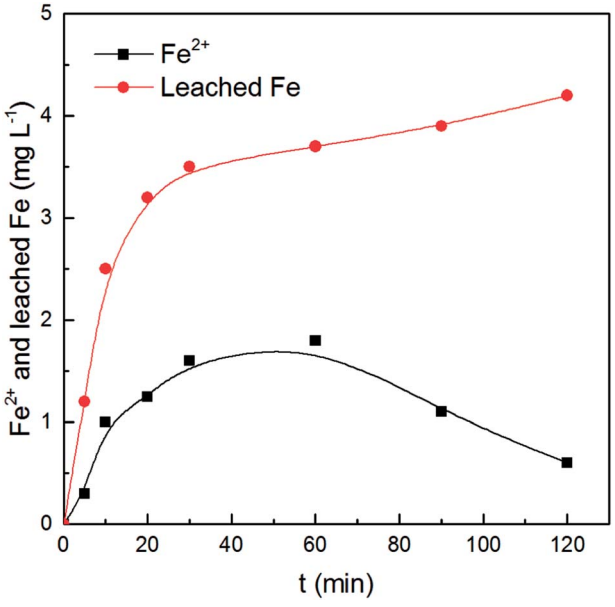

Fig. 6 Variation of the concentration of Fe^{2+} and leached Fe in the solution during CWPO of benzoic acid. Experimental conditions: 50 mg L^{-1} of benzoic acid, 1 g L^{-1} of catalyst, 250 mg L^{-1} of H_2O_2, T = 30 °C, pH = 3.2.

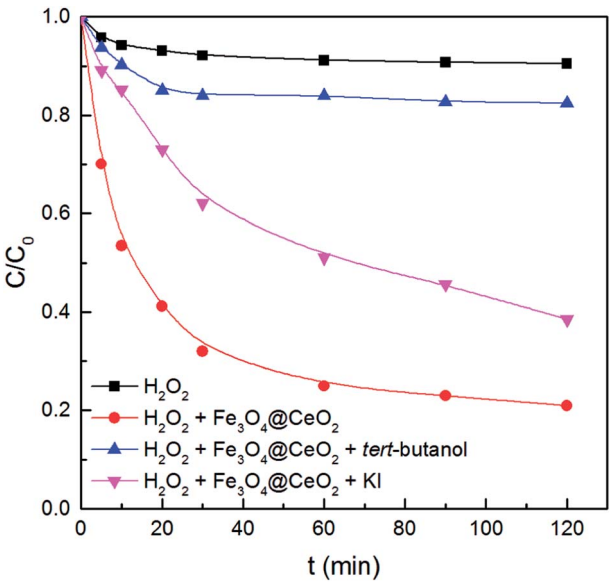

Fig. 7 Effect of radical scavengers on CWPO of benzoic acid. Experimental conditions: 50 mg L^{-1} of benzoic acid, 1 g L^{-1} of catalyst, 250 mg L^{-1} of H_2O_2, T = 30 °C, pH = 3.2.

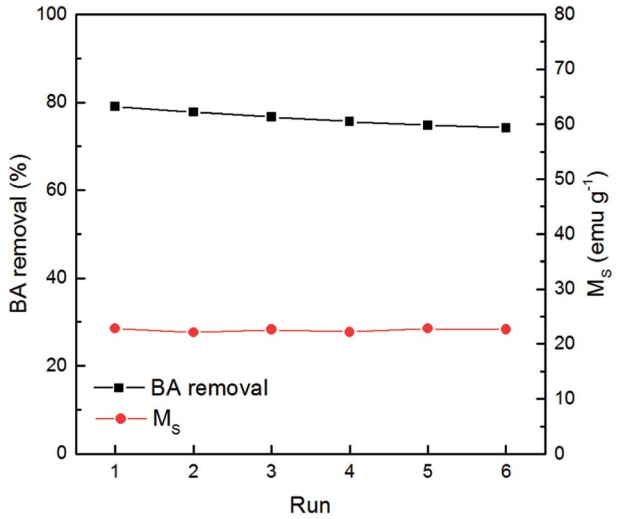

Fig. 8 Benzoic acid removal and the saturation magnetization of Fe_3O_4@CeO_2 catalyst in the stability tests. Experimental conditions: 50 mg L^{-1} of benzoic acid, 1 g L^{-1} of catalyst, 250 mg L^{-1} of H_2O_2, T = 30 °C, pH = 3.2.

Fe_3O_4@CeO_2 catalyst was subjected to successive degradation of benzoic acid six times. The used catalyst after each run was filtered out, washed with deionized water, and then dried at 110 °C for 24 h. As shown in Fig. 8, the removal rate of benzoic acid was reduced by merely 4% after six cycles of reaction. A slight loss of the used catalyst was inevitable during the recovery process. However, residual organic compounds adsorbed onto the catalyst might function negatively against its reusability.[28] Moreover, the saturation magnetization (M_s) of the catalyst before the reaction was 22.9 emu g^{-1}, and it remained almost unchanged after successive reactions. Overall, Fe_3O_4@CeO_2 was regarded as an excellent catalyst in terms of reutilization and stability.

4. Conclusions

Magnetic core–shell-structured Fe_3O_4@CeO_2 nanoparticles were successfully prepared, characterized, and systematically evaluated as a solid catalyst for CWPO of benzoic acid. Fe_3O_4@CeO_2 exhibited excellent catalytic performance for the degradation of benzoic acid. The excellent catalytic efficiency could be due to the synergistic effect between Fe_3O_4 and CeO_2, which enhanced the H_2O_2 decomposition into ·OH. In addition, it was found that Fe_3O_4@CeO_2 was highly effective for CWPO of benzoic acid in aqueous solutions at acidic and neutral pH. Compared to other previously reported results, the level of leaching Fe for Fe_3O_4@CeO_2 catalyst was very low. Based on the results of catalyst characterization and the effects of radical scavengers, a probable degradation pathway of benzoic acid by the attack of ·OH produced both in bulk solution and on the Fe_3O_4@CeO_2 surface was proposed. Fe_3O_4@CeO_2 was demonstrated to be an effective and stable catalyst in CWPO of benzoic acid in stability tests. In conclusion, Fe_3O_4@CeO_2 shows great potential in the treatment of benzoic acid-containing wastewater due to its catalytic and magnetic properties.

Conflicts of interest

There are no conflicts to declare.

Acknowledgements

The authors would like to convey their gratitude for the financial support from Provincial Key Disciplines of Chemical Engineering and Technology in Guizhou Province (No. ZDXK [2017] 8), Fund of Guizhou Department of Science and Technology (No. KY [2017] 1190 and KY [2017] 1187), United Fund of Guizhou Department of Science and Technology (No. LH [2017] 7317 and LH [2016] 7296), Fund of Tongren Department of Science and Technology (No. KY [2017] 36) and the Guizhou Provincial Department of Education Foundation (No. QJHKYZ2016-107).

References

1 X. D. Xin, W. Si, Z. X. Yao, R. Feng, B. Du, L. G. Yan and Q. Wei, Adsorption of benzoic acid from aqueous solution by three kinds of modified bentonites, *J. Colloid Interface Sci.*, 2011, **359**(2), 499–504.
2 D. M. Yang, Z. Q. Song and X. R. Qian, Adsorption of benzoic acid by hydrotalcites and their calcined products, *Environ. Eng. Sci.*, 2010, **27**(10), 853–860.
3 M. Koh and T. Nakajima, Adsorption of aromatic compounds on C_xN-coated activated carbon, *Carbon*, 2000, **38**(14), 1947–1954.
4 T. Velegraki and D. Mantzavinos, Conversion of benzoic acid during TiO_2-mediated photocatalytic degradation in water, *Chem. Eng. J.*, 2008, **140**(1), 15–21.
5 K. Mehrotra, G. S. Yablonsky and A. K. Ray, Macro kinetic studies for photocatalytic degradation of benzoic acid in immobilized systems, *Chemosphere*, 2005, **60**(10), 1427–1436.
6 M. I. Pariente, F. Martinez, J. A. Melero, J. A. Botas, T. Velegraki, N. P. Xekoukoulotakis and D. Mantzavinos, Heterogeneous photo-Fenton oxidation of benzoic acid in water: effect of operating conditions, reaction by-products and coupling with biological treatment, *Appl. Catal., B*, 2008, **85**(1), 24–32.
7 S. Esplugas, J. Gimenez, S. Contreras, E. Pascual and M. Rodríguez, Comparison of different advanced oxidation processes for phenol degradation, *Water Res.*, 2002, **36**(4), 1034–1042.
8 N. Azbar, T. Yonar and K. Kestioglu, Comparison of various advanced oxidation processes and chemical treatment methods for COD and color removal from a polyester and acetate fiber dyeing effluent, *Chemosphere*, 2004, **55**(1), 35–43.
9 C. Catrinescu, C. Teodosiu, M. Macoveanu, J. Miehe-Brendle and R. Le Dred, Catalytic wet peroxide oxidation of phenol over Fe-exchanged pillared beidellite, *Water Res.*, 2003, **37**(5), 1154–1160.
10 J. A. Melero, F. Martínez, J. A. Botas, R. Molina and M. I. Pariente, Heterogeneous catalytic wet peroxide oxidation systems for the treatment of an industrial pharmaceutical wastewater, *Water Res.*, 2009, **43**(16), 4010–4018.

11 A. Rey, M. Faraldos, J. A. Casas, J. A. Zazo, A. Bahamonde and J. J. Rodríguez, Catalytic wet peroxide oxidation of phenol over Fe/AC catalysts: influence of iron precursor and activated carbon surface, *Appl. Catal., B*, 2009, **86**(1), 69–77.

12 A. Rey, A. Bahamonde, J. A. Casas and J. J. Rodríguez, Selectivity of hydrogen peroxide decomposition towards hydroxyl radicals in catalytic wet peroxide oxidation (CWPO) over Fe/AC catalysts, *Water Sci. Technol.*, 2010, **61**(11), 2769–2778.

13 G. Q. Gan, J. Liu, Z. X. Zhu, Z. Yang, C. L. Zhang and X. H. Hou, A novel magnetic nanoscaled Fe_3O_4/CeO_2 composite prepared by oxidation-precipitation process and its application for degradation of orange G in aqueous solution as Fenton-like heterogeneous catalyst, *Chemosphere*, 2017, **168**, 254–263.

14 H. Zhao, H. J. Cui and M. L. Fu, Synthesis of core-shell structured Fe_3O_4@α-MnO_2 microspheres for efficient catalytic degradation of ciprofloxacin, *RSC Adv.*, 2014, **74**(7), 39472–39475.

15 F. J. Cui, J. W. Shi, B. Yuan and M. L. Fu, Synthesis of porous magnetic ferrite nanowires containing Mn and their application in water treatment, *J. Mater. Chem. A*, 2013, **19**(1), 5902–5907.

16 L. Xu and J. Wang, Degradation of 2,4,6-trichlorophenol using magnetic nanoscaled Fe_3O_4/CeO_2 composite as a heterogeneous Fenton-like catalyst, *Sep. Purif. Technol.*, 2015, **149**, 255–264.

17 H. D. Qin, H. L. Chen, G. Yang, X. M. Zhang and Y. J. Feng, Efficient degradation of fulvic acids in water by catalytic ozonation with CeO_2/AC, *J. Chem. Technol. Biotechnol.*, 2014, **89**(9), 1402–1409.

18 H. D. Qin, Q. Z. Dong, H. L. Chen, G. Yang and X. M. Zhang, Kinetics and mechanism of humic acids degradation by ozone in the presence of CeO_2/AC, *Ozone: Sci. Eng.*, 2015, **37**(4), 1–8.

19 H. D. Qin and H. L. Chen, Pretreatment of concentrated leachate by the combination of coagulation and catalytic ozonation with Ce/AC catalyst, *Water Sci. Technol.*, 2016, **73**(3), 511–519.

20 T. Montini, M. Melchionna, M. Monai and P. Fornasiero, Fundamentals and applications of CeO_2-based materials, *Chem. Rev.*, 2016, **116**(10), 5987–6041.

21 L. Xu and J. Wang, Magnetic nanoscaled Fe_3O_4/CeO_2 composite as an efficient Fenton-like heterogeneous catalyst for degradation of 4-chlorophenol, *Environ. Sci. Technol.*, 2012, **46**(18), 10145–10153.

22 W. K. Chang, K. R. Koteswara and H. K. Cing, A novel core-shell like composite In_2O_3@$CaIn_2O_4$ for efficient degradation of methylene blue by visible light, *Appl. Catal., A*, 2007, **321**(1), 1–6.

23 K. Maeda, N. Sakamoto, T. Ikeda, H. Ohtsuka, A. Xiong, D. Lu, M. Kanehara, T. Teranishi and K. Domen, Preparation of core-shell-structured nanoparticles (with a noble-metal or metal oxide core and a chromia shell) and their application in water splitting by means of visible light, *Chemistry*, 2010, **16**(26), 7750–7759.

24 S. Li, Y. H. Lin, B. P. Zhang, J. F. Li and C. W. Nan, $BiFeO_3$/TiO_2 core-shell structured nanocomposites as visible-active photocatalysts and their optical response mechanism, *J. Appl. Phys.*, 2009, **105**(5), 238–244.

25 Q. Wang, Y. Li, B. Liu, Q. Dong, G. Xu, L. Zhang and J. Zhang, Novel recyclable dual-heterostructured Fe_3O_4@CeO_2/M (M = Pt, Pd and Pt-Pd) catalysts: synergetic and redox effects for superior catalytic performance, *J. Mater. Chem. A*, 2014, **3**(1), 139–147.

26 S. T. Xing, Z. C. Zhou, Z. C. Ma and Y. S. Wu, Characterization and reactivity of $Fe_3O_4/FeMnO_x$ core/shell nanoparticles for methylene blue discoloration with H_2O_2, *Appl. Catal., B*, 2011, **107**(3), 386–392.

27 M. Kruk and M. Jaroniec, Gas adsorption characterization of ordered organic-inorganic nanocomposite materials, *Chem. Mater.*, 2001, **13**(10), 3169–3183.

28 H. D. Qin, R. Xiao and J. Chen, Catalytic wet peroxide oxidation of benzoic acid over Fe/AC catalysts: effect of nitrogen and sulfur co-doped activated carbon, *Sci. Total Environ.*, 2018, **626**, 1414–1420.

29 K. Y. Li, Y. Q. Zhao, C. S. Song and X. W. Guo, Magnetic ordered mesoporous Fe_3O_4/CeO_2 composites with synergy of adsorption and Fenton catalysis, *Appl. Surf. Sci.*, 2017, **425**, 526–534.

30 P. C. C. Faria, D. C. M. Monteiro, J. J. M. Orfao and M. F. R. Pereira, Cerium, manganese and cobalt oxides as catalysts for the ozonation of selected organic compounds, *Chemosphere*, 2009, **74**(6), 818–824.

31 P. C. C. Faria, J. J. M. Orfao and M. F. R. Pereira, Activated carbon and ceria catalysts applied to the catalytic ozonation of dyes and textile effluents, *Appl. Catal., B*, 2009, **88**(3), 341–350.

32 M. L. Luo, D. Bowden and P. Brimblecombe, Catalytic property of Fe-Al pillared clay for Fenton oxidation of phenol by H_2O_2, *Appl. Catal., B*, 2009, **85**(3), 201–206.

33 J. Y. Feng, X. J. Hu and P. L. Yue, Discoloration and mineralization of orange II using different heterogeneous catalysts containing Fe: a comparative study, *Environ. Sci. Technol.*, 2004, **38**(21), 5773–5778.

34 E. G. Heckert, S. Seal and W. T. Self, Fenton-like reaction catalyzed by the rare earth inner transition metal cerium, *Environ. Sci. Technol.*, 2008, **42**(13), 5014–5019.

35 R. C. C. Costa, F. C. C. Moura, J. D. Ardisson, J. D. Fabris and R. M. Lago, Highly active heterogeneous Fenton-like systems based on Fe^0/Fe_3O_4 composites prepared by controlled reduction of ironoxides, *Appl. Catal., B*, 2008, **83**(1), 131–139.

36 X. B. Hu, B. Z. Liu, Y. H. Deng, H. Z. Chen, S. Luo, C. Sun, P. Yang and S. G. Yang, Adsorption and heterogeneous Fenton degradation of 17α-methyltestosterone on nano Fe_3O_4/MWCNTs in aqueous solution, *Appl. Catal., B*, 2011, **107**(3), 274–283.

37 W. Luo, L. H. Zhu, N. Wang, H. Q. Tang, M. J. Cao and Y. B. She, Efficient removal of organic pollutants with magnetic nanoscaled $BiFeO_3$ as a reusable heterogeneous Fenton-like catalyst, *Environ. Sci. Technol.*, 2010, **44**(5), 1786–1791.